Check for updates

MRS FELLOWS FOCUS

Advances in the measurement of hardness at high strain rates by nanoindentation

B. L. Hackett[1], P. Sudharshan Phani[2], C. C. Walker[1], W. C. Oliver[3], G. M. Pharr[1,a]

[1] Department of Materials Science & Engineering, Texas A&M University, College Station, TX 77843, USA
[2] International Advanced Research Centre for Powder Metallurgy & New Materials (ARCI), Balapur P.O., Hyderabad, Telangana 500005, India
[3] KLA Corporation, 105 Meco Ln, Oak Ridge, TN 37830, USA
[a] Address all correspondence to this author. e-mail: pharr@tamu.edu

A new testing system and techniques for measuring the hardness of materials subjected to very high indentation strain rates up to 10^4 s^{-1} is presented. This was accomplished by modifying the components of a conventional nanoindentation system with a laser interferometer that records indenter displacements at 1.25 MHz. Using specially developed analysis techniques based on Newton's laws, these displacements can be converted to synchronous measurements of the indentation load, providing for the determination of indentation load–depth curves from which the hardness can be obtained. The testing system has been used to explore the behavior of two materials at opposite ends of the hardness spectrum—hard fused silica and soft single crystalline (111) aluminum. Results show that the hardness of fused silica is relatively insensitive to strain rate, whereas the hardness of aluminum at high strain rates (10^3–10^4 s^{-1}) increases by 25% compared to quasistatic testing.

Introduction

Nanoindentation has established itself as a powerful and versatile mechanical testing tool that can be applied across a wide variety of applications [1–5]. The unique utility of nanoindentation lies in its ability to controllably probe the mechanical properties of materials on length scales in the micrometer and sub-micrometer regimes. One emerging area of interest for new extensions of nanoindentation is the realm of high strain rate deformation. Conventionally, high strain rate testing is performed on macroscopic samples [6–10] by techniques such as plate impact [7], high velocity gas gun impact [8], split Hopkinson pressure bar testing [9], and laser shock testing [10]. Although standards in the field, these techniques generally require complex testing systems that limit the number of tests that can be performed on a given material in a given period of time. If successfully developed, high strain rate nanoindentation could potentially be developed into a high-throughput testing technique that could enormously accelerate testing times and significantly reduce costs.

In contrast to the large body of work on quasistatic nanoindentation, nanoindentation at high strain rates has been addressed only in a limited number of very recent studies [11–16]. This is partly due to the technical challenges in measuring indentation loads and displacements at fast enough acquisition rates at sub-micrometer scales. The earliest applications of conventional indentation testing to study dynamic material behavior circumvented the issue of direct measurement of loads and displacements by means of simple drop impact experiments [17, 18]. In these methods, the rebound height or velocity change of an impacting indenter is related to the initial drop height, the impact velocity, and the volume of deformed material in the hardness impression to arrive at a "rebound hardness," analogous to the statically determined hardness [17, 18]. Although initially developed for testing at the macro-scale, this type of test has recently been extended into the micro- and nano-regimes using laser ablation techniques to propel micron-scale hard particles launched to high velocities that impact the specimen at strain rates as high as 10^8 s^{-1} [19].

Other early methods for measuring hardness at high strain rates focused on directly measuring the forces and displacements during impact by an indenter of known geometry. The measurements of force were usually obtained by implementation of piezoelectric load cells in the testing systems [20–22], and indenter displacements were measured using strain gauges on

deflecting beams [23] or by Moiré interferometry [24]. Nanoindentation systems and testing techniques aimed specifically at the measurement of high strain rate mechanical properties at smaller scales have emerged based upon similar principles, including a pendulum-based system with capacitive displacement measurement [11–13], an instrument with a displacement-controlled piezoelectric actuator with an independent piezoelectric load cell [14], and a conventional nanoindenter adapted for use at higher than normal strain rates [15, 16]. Together, these studies have paved the way for achieving the time resolution, signal-to-noise ratio, dynamic instrument parameters, and measurement time constants needed to measure hardness at small scales at indentation strain rates up to 10^3–10^4 s^{-1}.

In this work, a new high strain-rate nanoindentation system based on the modification of conventional nanoindenter components along with refined methods for making hardness measurements and processing the data are used to explore the high strain rate hardness of two representative materials—hard fused silica and soft single crystalline (111) aluminum. The work is a natural extension of the testing methods developed by Sudharshan Phani and Oliver [15], who did their work with a conventional nanoindentation testing system, but differs in that the new testing system was specifically designed to improve on their results. The methods employed by Sudharshan Phani and Oliver utilize special data analysis techniques based on Newton's laws of motion and a precise knowledge of the dynamics of the testing system to convert the measured displacements to synchronous measurements of the indentation load. With a greatly enhanced displacement data acquisition rate of 1.25 MHz achieved by replacing the conventional capacitance displacement measurement gauge by a laser interferometer with a displacement resolution of ~ 10 pm, the new testing system greatly enhances the capabilities of the approach. Additional technical improvements in the new testing system include a higher load frame stiffness, a flexible hexapod specimen stage, and reduced internal resonances in the force actuator due to removal of the capacitance gauge. These improvements provide accurate indentation load–depth curves for tests lasting just a few hundred microseconds, and from which the hardness can be derived from nanoindentations with total penetration depths on the order of a micrometer or less.

We begin the presentation with a description of the instrument and the simple single-degree-of-freedom model used to accurately describe its dynamics. The model is then used to develop a new testing method based on an impact experiment in which the indenter starts from a specific distance off the specimen surface, accelerates toward the surface under a step force load, and impacts the specimen at maximum velocity and kinetic energy. This is in contrast to the step load procedure used by Sudharshan Phani and Oliver [15]. Special data reduction and filtering strategies are then used to calculate the

load on the sample from the dynamic model. Using the new techniques, values of the hardness at high indentation strain rates (10^3–10^4 s^{-1}) are measured for fused silica and (111) single crystalline aluminum as a function of time and indenter penetration depth for comparison to quasistatic measurements. The potential shortcomings of the technique and sources of error are evaluated, and implications of indentation size effects on the observations are discussed.

Experimental methodology

Instrumentation

The new high strain rate nanoindentation testing system is based on an InForce 1000 nanoindentation actuator head (KLA Instruments, Oak Ridge, TN) that provides up to 1 N of indenter force through an electromagnetic coil and magnet assembly. As shown in Fig. 1, the actuator was modified by removing the capacitive displacement gauge normally used to measure indenter displacement and replacing it with a laser interferometer (SmarAct GmbH, Oldenburg, Germany) that operates with ~ 10 pm displacement resolution at a data acquisition rate of 1.25 MHz, thus increasing the time resolution of the displacement measurement by more than an order of magnitude. The laser is directed through the center of the hollow loading shaft to the back of the indenter tip, where a mirror reflects it back to the laser system for analysis, with a delay time of about 1 μs. Accordingly, displacement is measured right at the sample, which reduces some of the machine compliance issues. To further reduce the machine compliance, a very stiff hexapod stage (Physik Instrumente, Karlsruhe, Germany) with a stiffness of 1×10^8 N/m was used to mount and position the sample, along with a very stiff
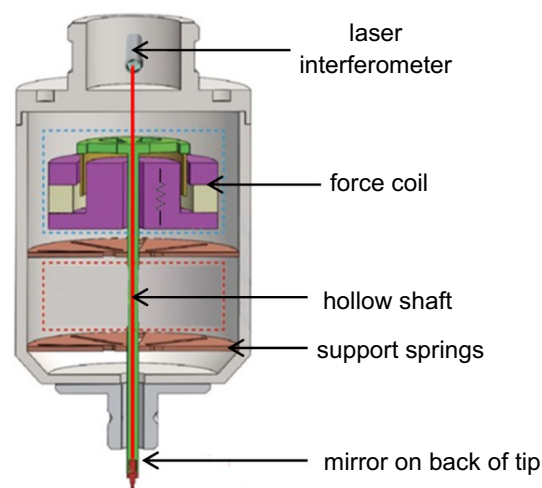

Figure 1: Modified InForce 1000 nanoindentation actuator used in the new high strain rate testing system.

gantry designed specifically for the system. The resulting machine stiffness, as measured by standard techniques [1], is 27×10^6 N/m, which is an order of magnitude larger than most commercial nanoindenters. This greatly simplifies some of the testing procedures and interpretation of the data. With three degrees of translational and three degrees of rotational freedom, the hexapod also provides for precision positioning and angular alignment of the specimen (± 0.5 μm). The system is also capable of performing quasistatic tests for direct comparison to the high strain rate results.

The basic method of operation of the instrument involves applying a current to the electromagnetic coil to achieve a prescribed force–time history and then measuring the indenter displacement as a function of load and/or time. The focus in this work will be on a step load force, F_o, referred to here as the "coil force." In this regard, it is important to note that during step loading, the load is not fully applied instantaneously, but rather is limited by the time constants of the mechanical and electrical components of the actuator. For the InForce 1000 actuator, the standard time constant, τ, is 300 μs, so the force increases with time, t, according to

$$F = F_o\left(1 - e^{-t/\tau}\right). \tag{1}$$

This is important because the loading times in high strain rate experiments are typically on the order of a few hundred microseconds, in which case the indentation force during a step load test is not constant but increases with time until it finally plateaus at the prescribed value. With the laser interferometer, the indenter displacement is measured at a sampling rate of 1.25 MHz, which provides the fine time resolution required for measurements at the indentation strain rates of interest (10^3–10^4 s^{-1}). As will be discussed shortly, the primary experiment performed with the instrument is a special step load impact test in which the indenter starts at prescribed distance off the surface, a step load is applied to accelerate it to the surface, and it then penetrates the material and elastically rebounds from it. Among other things, this procedure eliminates issues with the loading time constant.

All experiments were performed with a sharp Berkovich triangular pyramidal indenter to assure that small indentations could be produced and to take advantage of its geometric self-similarity. For the Berkovich indenter, the indentation strain rate is conveniently defined as [25]

$$\dot{\epsilon}_i = \dot{h}/h, \tag{2}$$

where h is the depth of penetration relative to the surface of the specimen and $\dot{h}$ is its first time derivative, i.e., the indenter velocity, v.

Dynamic model for the instrument

The dynamics of the instrument in response to an applied coil force are crucial to the high strain rate measurements since the measured displacement–time behavior during a test depends on both the mechanical properties of the specimen and the dynamics of the testing system. With the modified InForce 1000 actuator, the system dynamics can be accurately modeled using a single degree-of-freedom damped harmonic oscillator [15]. The model accounts for all the principal forces acting on the indenter, with the applied coil force counteracted by the inertia of the accelerating mass, the system damping (mostly due to eddy currents in the coil and magnet assembly), and the stiffness of the springs that support the indenter column. For a step load of magnitude F_o and the indenter hanging freely in air (i.e., not contacting the specimen), the differential equation describing the motion of the column is

$$m\ddot{h} + b\dot{h} + kh = F_o\left(1 - e^{-t/\tau}\right), \tag{3}$$

where m is the mass of the moving column and all that is attached to it, b is the system damping coefficient, and k is the net spring stiffness. In order to determine the constants m, b, and k, two separate approaches were used. The first was to apply a 10 mN step force F_o to the coil with indenter hanging freely in air to obtain the displacement–time data shown in Fig. 2. For this case, a closed form solution of the differential equation exists [26], which can be fit to the experimental data to determine the three machine constants, as illustrated in the figure. The second approach was a sinusoidal dynamic frequency sweep of the coil force, which is a standard calibration procedure used in nanoindentation testing [27]. The parameters from the displacement–time fit from the step load in air and those found
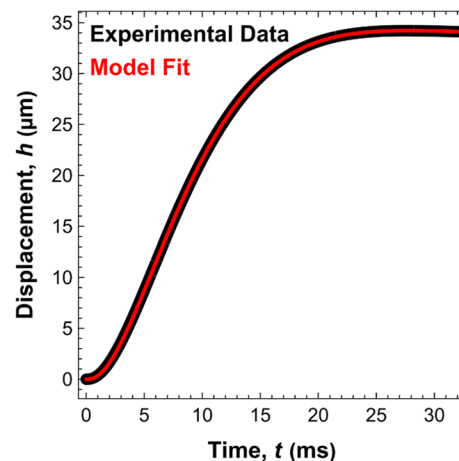

Figure 2: Indenter displacement vs. time for a 10 mN step load test in air from which the dynamic machine parameters were determined. The red line through the data is a fit obtained from the closed form solution of the differential equation.

TABLE 1: Dynamic instrument parameters.

Fit	m (g)	b (N · s/m)	k (N/m)
Step force	7.883	2.444	293.0
Dynamic sweep	7.793	2.466	294.6

by the dynamic frequency sweep are shown in Table 1, where it is apparent that the two methods give parameters within 1% of each other. For this work, the parameters from the first method were preferred because the test used to obtain them closely mirrors the form of the tests performed on the specimens. The excellent agreement between the model and the experimental data shown in Fig. 2 validates the one degree-of-freedom harmonic oscillator model for the testing system and supports its use in using the measured displacements to synchronously calculate the load on the sample.

Test procedure

In many ways, the ideal high strain rate indentation test is one in which the strain rate is held constant during the test at a prescribed value. For the geometrically self-similar Berkovich indenter, and when the hardness is independent of depth, this is conveniently accomplished by performing the test at a constant value of $\dot{P}/P$, where P is the load on the specimen and $\dot{P}$ is the loading rate [28]. In some commercial testing systems, this is accomplished through feedback control of the load, which is easily accomplished when the indentation strain rates are less than about 10^2 s^{-1} [16]. However, at higher strain rates, this is frequently not possible due to the clock rate at which the feedback control loop is updated [16], which in the new system used here is 1000 Hz. Thus, to circumvent this issue, we have chosen to focus on another testing procedure—one which achieves very high strain rates but at the expense of the strain rate being variable during the course of the test.

The test procedure is outlined in Fig. 3. It is essentially an indentation impact test in which the indenter starts well off the surface and is accelerated toward it at a constant applied coil force, F_o. The test sequence begins by accurately locating the surface by advancing the indenter slowly at a constant velocity while monitoring the displacement and applied force. When the surface is contacted, the stiffness quickly rises and crosses a threshold set just above the stiffness of the indenter column springs. The absolute displacement associated with this contact is recorded, and displacement thereafter is referenced relative to that point. Since this surface detection procedure proceeds slowly, it very accurately indexes the surface location prior to high-rate impact testing and thus avoids problems in analyzing high velocity displacement–time data during the impact event that can lead to inaccuracies in defining the surface location.
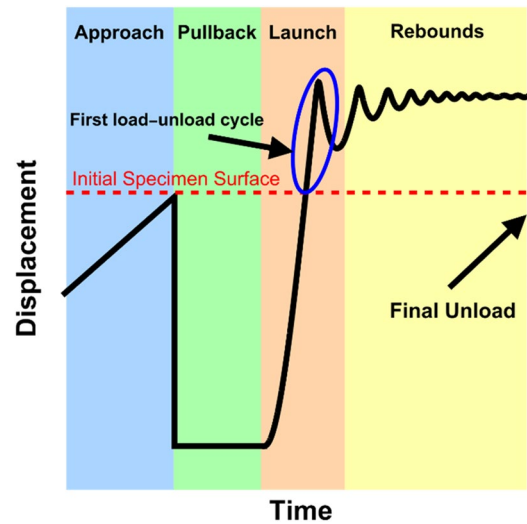

Figure 3: Schematic illustration of the impact test procedure. Note that the displacement and time in the figure are not to scale and only serve to illustrate the distinct regions.

It is noted that, as in quasistatic nanoindentation experiments, highly compliant materials may require extra care and procedural steps to ensure the surface location is properly determined while avoiding alteration of the surface prior to testing.

The second step in the testing procedure is to back up the indenter from the surface to a prescribed launching distance, h_o, which gives the maximum indenter velocity at the point of impact. As discussed and derived elsewhere based on the dynamics of the actuator [26], this distance is given by

$$h_o = (F_o/k)(1 - Z), \qquad (4)$$

where Z depends on the actuator parameters through

$$Z = \left(\tfrac{2}{1-X}\right)\left(\tfrac{1+X}{1-X}\right)^{-(1+X)/2X}; X = \sqrt{1 - 4mk/b^2}. \quad (5)$$

After pullback, the indenter is launched toward the specimen at a constant coil force, F_o, and strikes the surface at time, t_o, and maximum velocity, v_o, given by [26]

$$t_o = \left(\tfrac{m}{b}\right)\left(\tfrac{1}{X}\right)\left(\tfrac{1+X}{1-X}\right); v_o = F_o Z/b. \qquad (6)$$

After impacting the surface, the indenter elastically rebounds and goes into a state of damped oscillation, after which it is fully unloaded.

There are several advantages to impacting the specimen with the velocity at its maximum. These include (1) minimization of transient effects caused by the loading time constant; (2) optimization of kinetic energy transfer so as to give the maximum force and penetration depth; (3) simplification of the mathematics used to analyze the data and compute the dynamic forces; and (4) reduction of acceleration uncertainty error [26]. To briefly

elaborate on these, having the indenter impact the sample after a set amount of time bypasses complications that arise from the initially rising coil force due to its time constant, τ. At $t = 5\tau$, the force applied by the coil reaches 99.3% of the target F_o value, and therefore the time dependency of the force application can be neglected for $t > 5\tau$. For the instrument parameters in Table 1, the time to reach the sample for the maximum velocity at impact is constant at approximately 5.8 ms (19.33τ) for all F_o at the proper backup distance, and this satisfies the $t > 5\tau$ requirement. Another reason for implementing maximum velocity at impact is that the maximum velocity produces the maximum amount of kinetic energy available to be transferred to the sample for a given step force magnitude, thus producing the largest amount of dynamic overload for a given step load magnitude. As discussed in detail elsewhere [26], this also greatly simplifies the mathematics describing the formation of the contact for a self-similar indenter. Since the maximum velocity condition implies that the indenter acceleration is zero at the time of first contact, the kinetic energy of the indenter column is exactly balanced by the work done on the material as the indentation contact impression is formed, which results in $h(t)$ being expressible in a closed analytical form, following a few simplifications [26]. It is also notable that the maximum velocity condition minimizes the uncertainty in acceleration, and this helps to minimize the error in the inertial force contribution to the calculation of the net force on the sample by means of the dynamic considerations described in the next section.

It is useful to note that the expressions for the pullback distance and maximum velocity given in Eqs. 4 and 6 reduce to a simple linear proportionality with respect to F_o. This means that the velocity, or likewise the kinetic energy at impact ($mv^2/2$), can be proportionally controlled by varying F_o. For the dynamic parameters given in Table 1, the critical pullback distance simplifies to

$$h_o = [1091 nm/mN] \times F_o, \tag{7}$$

and the maximum velocity at impact is

$$v_o = [0.2782 mm/(s \cdot mN)] \times F_o. \tag{8}$$

In Fig. 4, the velocity of the indenter traveling through air in response to a coil force $F_o = 10$ mN is shown to compare experimental measurements to the solution of dynamic instrument model of Eq. 3. It is notable that the model closely agrees with the data even after differentiation with respect to time to obtain the velocities. According to Eq. 8, the maximum velocity in this case is 2.782 mm/s. Since the InForce 1000 actuator is capable of applying 1000 mN of force, the absolute maximum velocity achievable in the new system is limited to 278 mm/s. Thus, the high indentation strain rates achieved in the tests result mostly from the small depths of penetration rather than high impact velocities (see Eq. 2).
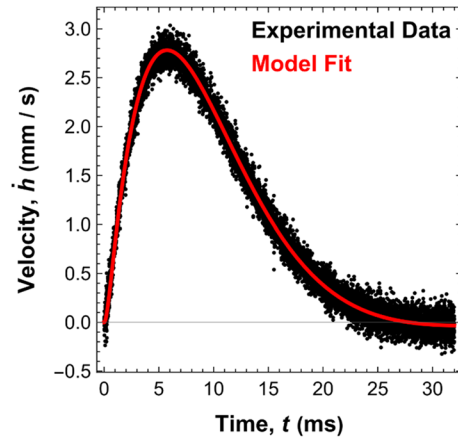

Figure 4: Comparison of the velocity–time response of the dynamic model to experimental data for an experiment conducted in air at $F_o = 10$ mN. $t \approx 5.8$ ms corresponds to the maximum velocity.

Note that since the velocities are much less than the speed of sound, there is no need to incorporate the influences of elastic wave propagation in the analyses. No stress wave effects were experimentally observed.

Load measurement

During the course of experimenting with the new system, it was discovered that there are several important issues related to the synchronization of the load and displacement measurements, and one way to minimize these problems is to calculate the load on the sample at a given time directly from the measured displacements and application of Newton's laws of motion, as originally proposed by Sudharshan Phani and Oliver [15]. The additional contribution of the resistance of the sample can be included by adding a term to Eq. 3 for the load, P, applied to the sample (or equivalently, the load applied by the sample to the indenter column), which after rearrangement yields

$$P = F_o\left(1 - e^{-t/\tau}\right) - m\ddot{h} - b\dot{h} - k(h + h_o). \tag{9}$$

Note that when written this way, the zero of displacement is taken at the sample surface, so the force applied by the springs must be adjusted to account for the backup distance h_o.

It follows from Eq. 9 that if the displacement–time data is of high enough quality and resolution to accurately obtain the first and second time derivatives, i.e., the velocity, v, and acceleration, a, then the load on the sample can be computed from the displacement data alone, and there will be no issues concerning their synchronization. However, high-frequency noise in the data complicates accurate calculation of the derivatives, and as a result, the displacement data must first be carefully smoothed and filtered, as discussed in the next section. It should be noted

that at no time in the analysis procedure is a constitutive relation for the material assumed a priori.

Using these procedures, the displacement–time and derived load–time curves for an impact test in fused silica are shown in Fig. 5, where the zero for time starts at the instant when the launching force is stepped to 10 mN. As the indenter accelerates toward the surface after having been backed up the requisite distance, it reaches the maximum velocity as it contacts the surface. The material then begins to deform elastically and plastically, and the load on the sample and depth of penetration rise until a peak load is achieved. Subsequently, the indenter elastically rebounds and unloads, and as the load on the sample returns to zero, the indenter loses contact. Since the load applied by the coil remains constant, this is then followed by several elastic loadings and unloadings that damp away with time until a final equilibrium load and depth are achieved. Note that although the applied coil force is 10 mN, the maximum dynamic force reached in the impact is nearly 100 mN. Thus, the dynamic overload under these conditions is nearly a factor of 10.
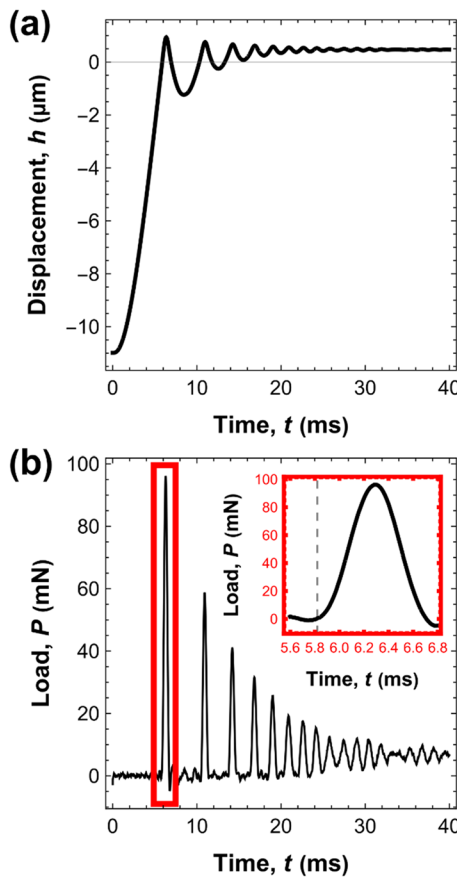

Figure 5: (a) Displacement–time and (b) calculated load–time behavior during a 10 mN coil force impact test of fused silica subject to the condition of maximum velocity at first contact. The inset in (b) details the P–t response during the first loading and unloading of the indenter into the specimen.

Data processing

The paramount importance of smoothing and filtering the displacement–time data prior to evaluating the derivatives is illustrated in Fig. 6, which presents experimental results from an impact test in fused silica at a coil force of 10 mN. The data include the first loading after contact with the specimen and the first unloading. In the upper row of results, the displacement–time data (left-hand side) have been differentiated by cubic spline fitting to give the velocity–time response (center), and this in turn has been differentiated again by cubic splines to give the acceleration–time response (right). What is not apparent in the displacement–time data is that it contains high-frequency noise on the order of ± 1 nm. This noise shows up distinctly in the calculated velocities, and it is so large in the accelerations that the measurements are essentially useless.

To correct for this, a low-pass Fourier filter was applied to filter out the high-frequency noise using procedures outlined in the "Materials and methods" section. The data after filtering are shown in the bottom row of Fig. 6, where there is striking transformation of the data into a usable form. We note, however, that it is imperative that the effects of the filter be well understood, since the filtering itself can introduce spurious artifacts. The main downside of implementing the low-pass filter is it that it can introduce features in the data that artificially influence the acceleration and hence the calculated load on the sample, especially at the beginning and end of contact and at maximum load. These undesirable filtering artifacts are larger the closer the low-pass cutoff frequency is to the fundamental frequency of the indentation contact event. Thus, filtering is an essential step for subsequent data analysis, but care must be taken in its application.

Hardness calculation

Hardness in a nanoindentation test is conventionally determined from the peak indentation load, P, and projected contact area, A_c, using

$$H = P/A_c, \qquad (10)$$

where the projected contact area is computed from the contact depth, h_c, and the known area function of the indenter [27]. The peak load is usually a measured or applied quantity, and the contact depth is derived either from an analysis of the unloading curve or by measuring the contact stiffness by continuous stiffness measurement (CSM) techniques [1]. In this work, the primary objective was to determine how the hardness varies with strain rate during the course of the initial loading segment, for which the CSM technique would be ideal. However, CSM measurements rely on a small oscillation of the load with time which is not possible in the short time periods of contact during high strain rate testing. As an alternative, we choose here to
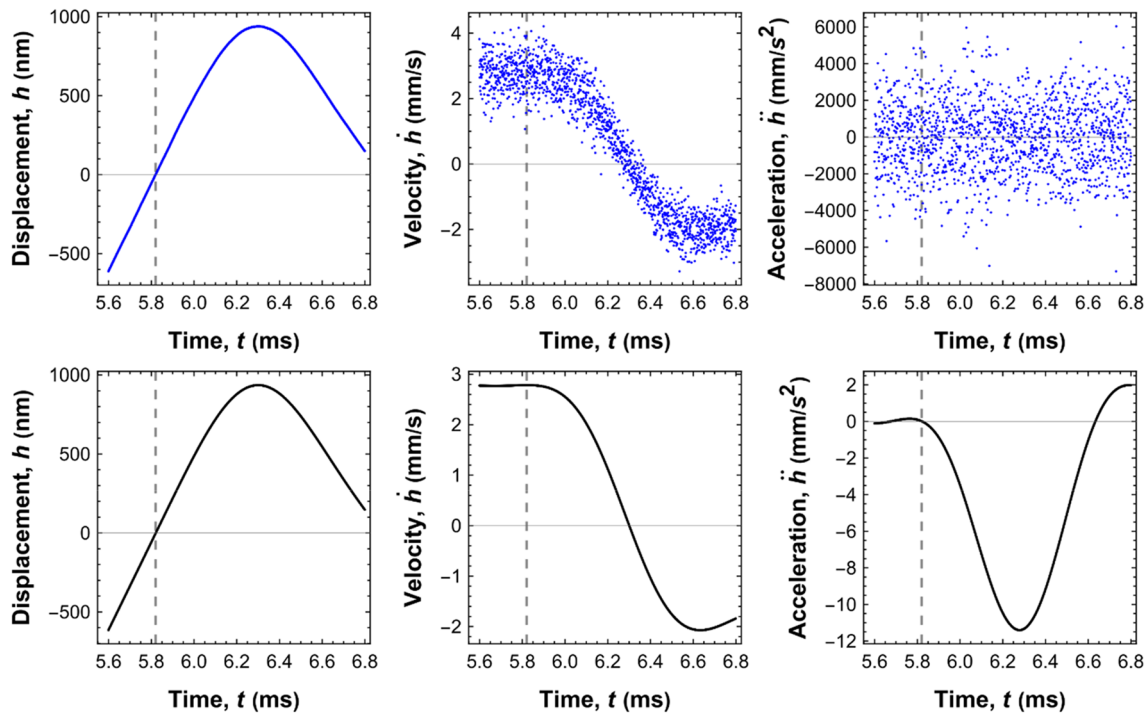
Figure 6: Effects of the low-pass Fourier filter on the components of the load on sample calculation without applying the filter (top row) and after applying the filter (bottom row). The displacement–time data were obtained in an impact experiment on fused silica using a coil force of 10 mN.

assume that the ratio of the contact depth to the total depth of penetration, h_c/h, is constant independent of depth, as is often the case in quasistatic tests conducted with the geometrically self-similar Berkovich indenter. This assumption is not totally valid when there is an indentation size effect and may not hold well in a highly strain rate-dependent material, effects that are currently under further investigation. However, for the purposes of development here, we assume that h_c/h is indeed a constant independent of depth and determine its value either from quasistatic measurements or by direct measurement of the dimensions of residual contact impressions using scanning laser microscopy (SLM) or atomic force microscopy (AFM) to measure the residual contact depths and contact areas.

Results and discussion

Indentation strain rates during impact testing

We begin the discussion by considering the strain rates achievable with the new testing system. Figure 7 shows how the measured indentation strain rate $\dot{h}/h$ varies with time and indentation depth during impact tests on fused silica and (111) Al for coil forces varying from 1 to 50 mN. The upper portion of the figure shows the relation between strain rate and time for the initial loading of the indenter into the specimen, with $t = 0$ corresponding to initial contact of the surface. The lower portion of the figure shows the same data

plotted as a function of the indentation depth, with both sets of plots using double logarithmic scales. Clearly, the strain rate is not constant but steadily decreases with time and depth as the indenter slows from its maximum velocity and zero acceleration condition at the beginning of the test to zero velocity and zero acceleration at the maximum penetration depth. The continuous deceleration is governed by the retarding forces generated by a contact of ever increasing size along with the damping and springs in the actuator. It is clear that the larger the applied coil force (and thus the kinetic energy of the indenter column), the deeper the penetration depth, as would be intuitively expected. On the other hand, the time of contact during loading decreases with increasing coil force because the indenter velocities are much greater. Accordingly, one has some control over the strain rates and penetration depths by varying the applied coil force. Note that the penetration depths for aluminum are larger than for fused silica due to the great difference in the hardness of these two materials.

One curious feature of the data in Fig. 7 is the convergence of the strain rates in the strain rate vs. time data (the upper plots) to a single line at shorter times. This is a direct consequence of striking the surface at zero acceleration along with the fact that at the smaller depths of penetration, and thus smaller times, the contact areas are exceedingly small. This means that the retarding force generated by the material is negligible in comparison to the coil
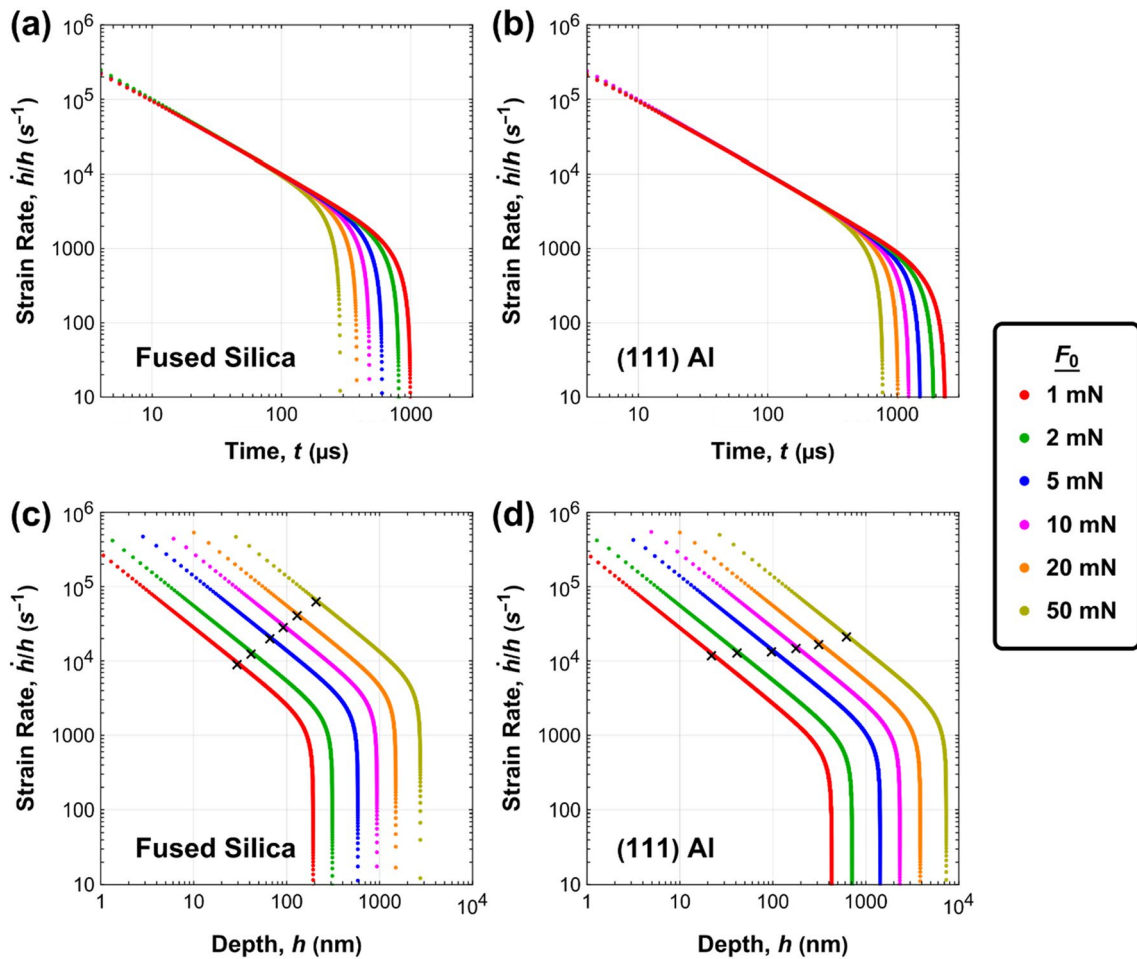
Figure 7: Variation of indentation strain rate with time (a, b) and indentation depth (c, d) during nanoindentation impact tests on fused silica and (111) Al. The coil forces F_o vary from 1 to 50 mN. The crosses (x) in (c) and (d) indicate the instrument strain rate cutoffs.

force F_o, which is initially balanced by the damping and spring forces in the actuator. Thus, until the contact area grows large enough that the resistance from the material is significant, the deceleration of the indenter column is very small, and its velocity remains essentially constant at v_o. Under these conditions, the differential equation describing the motion (Eq. 9) reduces to

$$F_o = b\dot{h} + k(h + h_o), \qquad (11)$$

and solving this simple equation yields that the indentation strain rate at short times and small depths is simply $\dot{h}/h = 1/t$. Inspection of the data in the upper portion of Fig. 7 bears this out for times up to about 100 ms for both fused silica and aluminum. For example, at $t = 10\ \mu s = 10^{-5}$ s, the strain rate is exactly 10^{+5} s^{-1} for both materials. This same phenomenon also explains why the shorter time data in the strain rate vs. depth plots in the lower portion of Fig. 7 are all parallel with a log–log slope of -1. Only when the contact area grows to produce a decelerating force large enough to influence the other forces does the behavior begin to deviate.

This is an important observation since it means that at small times and penetration depths, the experimentally observed behavior has nothing to do with the material and is controlled entirely by the machine dynamics. As a result, the measurements at these time and depth scales yield no information about the material. Put another way, since the net measured force is the sum of the force borne by the specimen and that borne by the machine, determining the force on the specimen requires subtracting the machine forces from the total measured forces. Consequently, if these two are essentially the same, the resulting computed force on the specimen will be subject to considerable error.

A detailed analysis of this has been developed elsewhere [26], where it is argued that estimates of the times and depths below which the specimen measurements are not trustworthy are determined by the uncertainty in the machine dynamic parameters m, b, and k. Assuming that these are known to no better than 1%, and that the maximum allowable error in the load on specimen and hardness calculations is 10%, this yields

the simple result that meaningful hardness data can be obtained only when $|F_{ins}/P| \leq 10$, where P is the actual load on the specimen and F_{ins} is the instrument contribution to the total measured force given by

$$F_{ins} = ma + bv + k(h + h_o). \tag{12}$$

This condition results in the "instrument strain rate cutoffs" shown in the lower part of Fig. 7, which correspond to the indentation depths below which any parameters derived from the measured load on the specimen such as the hardness are unreliable. After accounting for the strain rate cutoffs, it is apparent that the indentation strain rates at which hardness can be reliably measured under the testing conditions included in Fig. 7 are limited to the 10^4–10^5 s^{-1} range for fused silica and the 10^4 s^{-1} range for aluminum.

Load–depth curves

Using the procedures outlined in the previous sections, the loads borne by the sample during a maximum velocity impact test (zero acceleration at the point of contact) have been determined for tests conducted on fused silica and (111) Al, with the resulting load–depth curves for one cycle of loading and unloading at several coil forces F_o shown in Fig. 8. In general, all the impact test curves follow the same loading path, although there is some evidence in the aluminum data that increasing the coil force, and therefore the net strain rate, results in slightly higher loads. One noticeable feature is that the loading curves are not entirely smooth but rather undulate slightly, with the occurrence of undulations increasing as F_o increases. This is especially apparent in the aluminum data. These fluctuations are likely not real material behavior but rather a consequence of filtering. The low-pass Fourier filter inherently cuts out some important

frequencies that comprise the displacement–time response, and in the search to find a balance between noise reduction and signal fidelity, some noise below the cutoff frequency inevitably passes through. Consequently, the influences of some of the representative high frequencies of the true material response are diminished. This issue is further discussed in the "Materials and methods" section.

When compared to the quasistatic responses also shown in Fig. 8, it is clear that the high-rate behavior of fused silica and (111) aluminum is distinctly different. To first order, the loading curves for the impact tests in fused silica are all approximately the same as the quasistatic data, suggesting that this material is strain rate insensitive. On the other hand, the loading curves for the high-rate impact tests in aluminum are distinctly higher than the quasistatic test. This then suggests that aluminum exhibits some strain rate sensitivity, and there is thus a reason to believe the hardness at high strain rates will also be measurably increased.

The unloading curves for the two materials also show important differences, with the fused silica data suggesting there may be greater elastic recovery during the high strain rate testing. This is indirectly borne out in the scanning laser micrographs (SLM) of large hardness impressions shown in Fig. 9. Although the two aluminum indentations at low and high strain rates are very similar in appearance, the fused silica indentations are distinctly different in shape. Specifically, the fused silica indents created at high strain rates exhibit distinctly bowed-in sides [Fig. 9(a)], which is frequently an indicator of greater sink-in and therefore a greater degree of elasticity in the contact deformation. Note, however, that this interpretation may be influenced by the cracking that is readily apparent at the contact periphery.
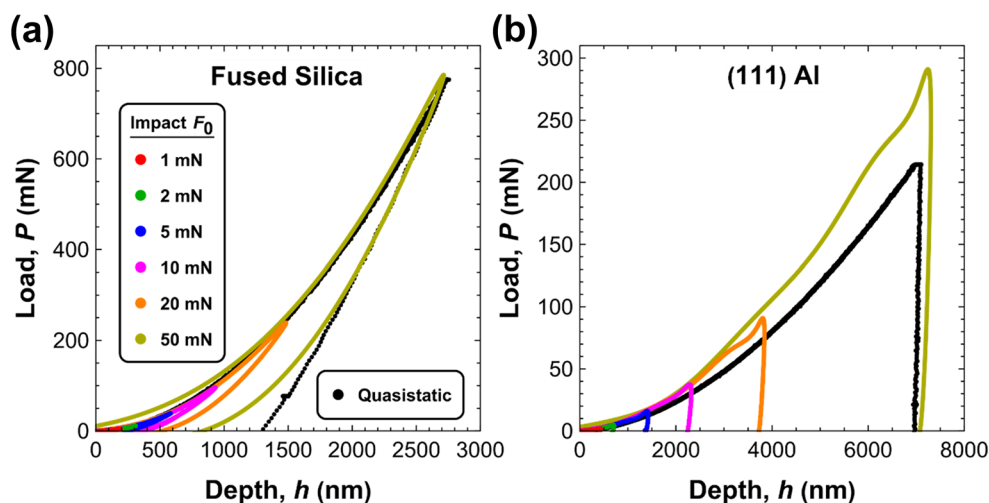

Figure 8: Load–depth curves for high strain rate indentation impact of (a) fused silica and (b) (111) Al for values of the applied coil force F_o in the range 1–50 mN. For comparison, results of a quasistatic test (black data points) obtained in the same testing system are also shown.
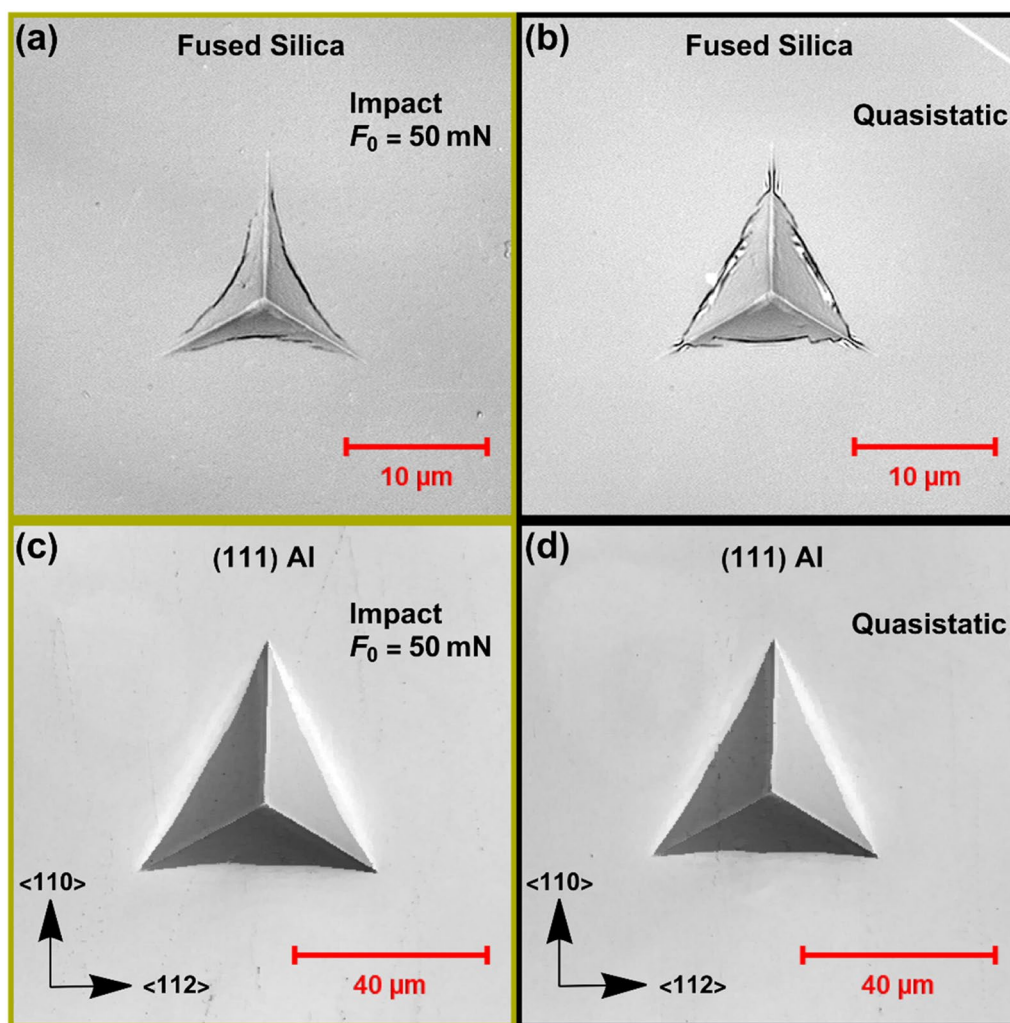
Figure 9: Scanning laser micrographs of the large load indentations for (a) impact tested fused silica, (b) quasistatically tested fused silica, (c) impact tested (111) Al, and (d) quasistatically tested (111) Al.

Rate effects on hardness

From the data used to generate the loading curves in Fig. 8, the depth dependence of the hardness was determined using the procedures developed in the "Hardness calculation" section which requires a value for the ratio of the contact depth to the total depth of penetration, h_c/h. Fused silica sinks in during quasistatic testing, so we assume the value determined from normal nanoindentation data analysis procedures, $h_c/h = 0.68$ [27], holds for both the quasistatic and impact tests. On the other hand, aluminum tends to pile-up during nanoindentation, and under these conditions the value of h_c/h measured by standard nanoindentation procedures may differ from the true value [29]. As a result, we choose a value that matches actual hardness measurements based on the projected contact areas measured at the end of loading determined by SLM. This gives $h_c/h = 0.92$, which is similar to the value $h_c/h = 0.98$

obtained from the quasistatic data, but different enough to be taken into account.

The resulting plots of hardness versus strain rate are shown in Fig. 10. The data in these plots below the instrument strain rate cutoff and a filtering cutoff discussed later have been excluded by showing it as grayed out in the figure. For the fused silica data in Fig. 10(a), the hardnesses for all the impact tests are very flat except those at the highest strain rates (> 5000 s^{-1}). In addition, the value of the hardness in the flat region is slightly greater than 9 GPa, which is very close to that observed in quasistatic testing. This suggests that for strain rates up to 5000 s^{-1}, fused silica is very strain rate insensitive. The slight upturn in hardness at the highest strain rates in some of the data is most likely a filtering artifact, as discussed at the end of this section.

On the other hand, the aluminum data in Fig. 10(b) are much more complex. Ignoring the undulations in the high strain
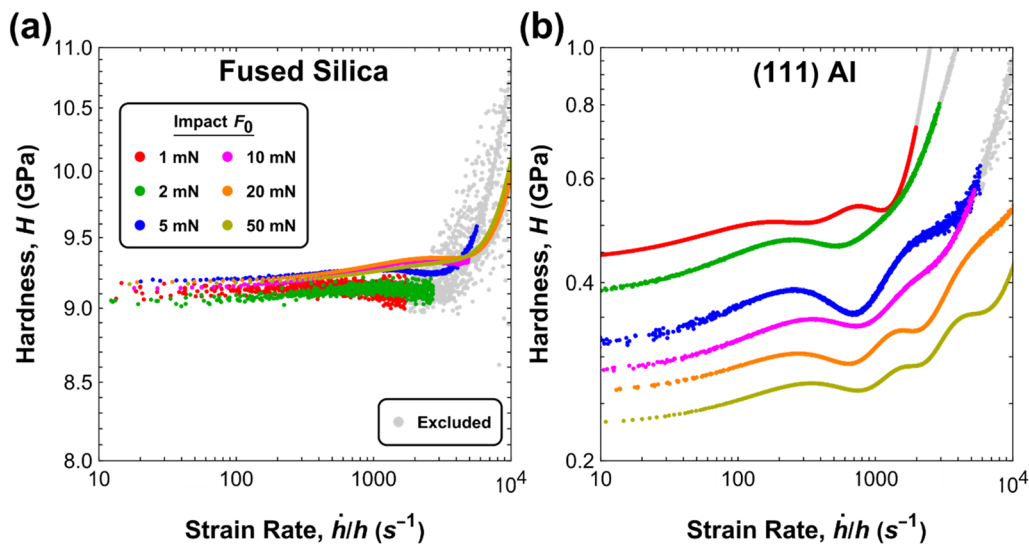
1172

Figure 10: Hardness as a function of strain rate for all the dynamic impact tests: (a) fused silica and (b) (111) Al.

data as a filtering artifact, there are two noteworthy features. First, the hardnesses measured in the impact tests show a tendency to increase with strain rate at high strain rates, suggesting the strain rate sensitivity may increase measurably for strain rates in excess of 10^3 s^{-1}. This behavior has also been observed in split Hopkinson bar experiments and may indeed be a real material effect [15]. Second, there is a distinct increase in the overall hardness as the applied coil force F_o decreases, which runs contrary to what one might expect based on the fact that larger values of coil force produce larger overall strain rates.

To understand this, the hardness data in Fig. 10 have been replotted as a function of indentation depth in Fig. 11.

Figure 11(b) for the aluminum data includes discrete plotting symbols which are hardnesses based on optical measurements of the residual contact area at the end of the test, both for the high strain rate data and at several different interrupted depths for the quasistatic data. The close agreement between the optically measured hardnesses and those derived from the depth–time data confirms the adequacy of the data analysis procedures. Interestingly, all the high-rate aluminum data roughly coalesce around a single curve, although there is a small but consistent increase in hardness with increasing coil force, as might be expected for a slightly strain rate sensitive material. However, the more important observation is that for the high-rate data
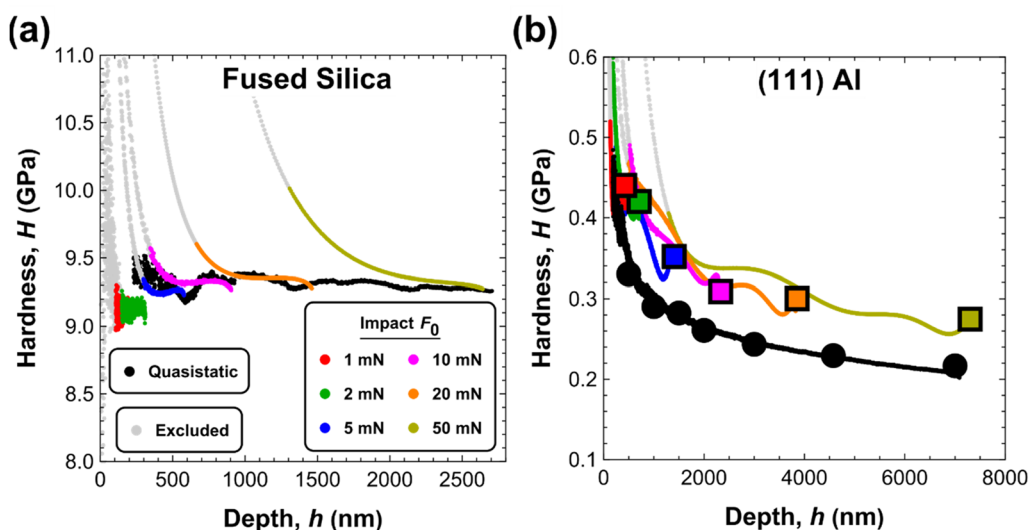

Figure 11: Hardness as a function of indentation depth for all the dynamic impact tests: (a) fused silica and (b) (111) Al. The discrete data points in the aluminum data indicate hardnesses derived from optically measured contact areas.

taken as a whole, the hardness decreases with increasing indentation depth, suggesting there is a high-rate "indentation size effect" similar to that observed in many metallic materials [30]. In fact, the same size effect is apparent in the quasistatic data, but at lower overall levels of hardness. Collectively, the data suggest that there are both size and rate effects in aluminum, with the rate effects manifested, to first order, as a simple vertical shift of the quasistatic data.

The data for fused silica in Fig. 11(a) generally corroborate the conclusion that fused silica is strain rate insensitive, with the exception of a slight upswing in hardness with decreasing penetration depth for each of the applied coil forces. However, we strongly suspect this upswing is not real but rather a filtering artifact. Filtering artifacts generally result in an overestimation of the load on the sample at the beginning of contact and become progressively worse for shorter durations of contact, corresponding to increases in F_o. This filter-induced error coincides with the time period of the highest strain rates, thus giving the false impression that there is a strong rate-dependent hardening effect. A telltale sign of the filtering artifact is that the calculated load is not zero at zero depth, as can be seen, for example, in the $F_o = 50$ mN data in Fig. 8(a). Indeed, it is this slightly positive load at zero depth that causes the artificial upswing in the calculated hardness.

The upswing in the calculated hardness caused by filtering can, in fact, be directly reproduced and quantified through simulation. To demonstrate this, a simple constitutive response for fused silica assuming a constant hardness with depth, that is, no indentation size effect, was used in conjunction with the differential equation modeling the experiment (Eq. 9) to generate a set of hardness vs. strain rate data. This was accomplished by replacing the load on the sample, P, in Eq. 9 with Ch^2, where the variation of P with h^2 assures a depth-independent hardness, as would be expected for the geometrically self-similar Berkovich indenter. The constant C was chosen to give the correct level of hardness for fused silica. After the differential equation was solved numerically for the depth–time response, the dataset was processed to obtain the depth dependence of the hardness using the same parameters and filtering procedures used in the experimental test. The results are shown in Fig. 12, where it is clear that even when there is no noise in the data, there is an upswing in hardness at shallow depths that matches well with the data from the real test, even though there is no small-depth upswing in the actual hardness as modeled.

To account for this in the experimental data obtained in this work, an additional data exclusion criterion was included in the strain rate cutoff. As in the analysis of the instrument strain rate cutoff, a 10% hardness deviation allowance was assumed, but the cutoff points were determined using the simulated effect of the filter for each test. This was done so as not to result in
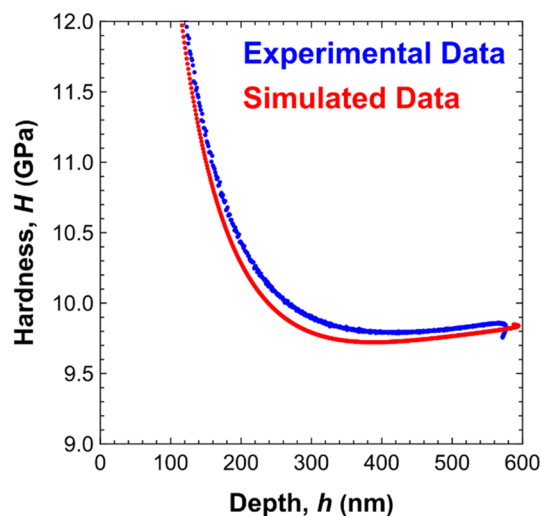

Figure 12: Simulated 5 mN fused silica impact data passed through the same filter as in the experimental tests showing that the small-depth upswing in hardness is likely caused by the filtering.

exclusion of data in materials that do indeed have real changes in hardness as a function of depth or strain rate. Although data in the excluded regions are most certainly wrongly influenced by instrument uncertainties and filtering artifacts, any abrupt change in hardness must be thoroughly scrutinized regardless of whether or not the change falls within an excluded zone.

Conclusions

The increased time resolution (1.25 MHz) from laser-measured displacement of a specially designed high strain rate nanoindentation testing system combined with a method for accurately and synchronously determining the indentation load by a dynamic analysis of the specimen and machine contributions to the forces during contact has been developed to provide an enhanced capacity to measure hardness at high strain rates during nanoindentation testing at small length scales. Using fused silica and a (111) single crystal of aluminum as model materials at the extremes of the hardness scale, it was shown that the new testing system is capable of producing indentation strain rates up to or greater than 10^4 s^{-1} during a specially designed impact test in which the indenter velocity is maximized at the point of first contact. This results in a maximum kinetic energy transferred to the material to form the hardness impression, which then produces high indentation strain rates and maximum depths of penetration. Although the maximum indenter velocity in the new testing system is limited to about 0.3 m/s by the maximum force the actuator can apply (~ 1 N), high indentation strain rates can be achieved as a result of the small penetration depths over which the measurements are made. The merits and limitations

of the new system and testing methodology were evaluated by making dynamic hardness measurements in fused silica and (111) aluminum. The load on sample, strain rate, and hardness were all computed by solving a system-governing differential equation based on Newton's laws of motion in conjunction with precise experimental measurements of indentation depth vs. time and well-calibrated parameters describing the dynamics of the testing system. Low-pass Fourier filtering was found to be crucial for data analysis and processing, with limits on the achievable strain rate set by uncertainties in machine dynamic parameters and data filtering. Varying the force applied by the actuator, F_o, and the distance, h_o, to which the indenter is backed up from the surface prior to impact allows some control over the strain rates and depth ranges that can be achieved.

The hardness of (111) Al was found to be strain rate sensitive, with high strain rate impact testing producing hardnesses ~ 25% greater than those in quasistatic testing. In addition, a distinct indentation size effect was observed for aluminum during both high strain rate and quasistatic testing, with the findings confirmed by optical measurements of the hardness impressions after indentation. On the other hand, the hardness of the fused silica exhibits virtually no strain rate sensitivity or size effects, although there is some evidence based on optical microscopy of the hardness impressions that the contact geometries are distinctly different at low and high strain rates.

This work provides a foundation for future efforts focusing on material-related effects during high strain-rate nanoindentation testing, with the possibility of developing the techniques into high-throughput and low-cost methods for assessing mechanical behavior at high strain rates.

Materials and methods

Materials and nanoindentation test parameters

Two materials were tested in this study—a high-purity (111) aluminum single crystal (Surface Preparation Laboratory, Netherlands) and fused silica (Corning, USA), both in the form of highly polished (0.05 μm colloidal silica) 10 mm × 3 mm circular disks. The two materials were chosen to highlight the differences between very soft and very hard materials. Both have an elastic modulus, E, of about 70 GPa. Single crystalline aluminum was selected in favor of polycrystalline to avoid grain boundary influences on the measurements and eliminate effects of grain-to-grain elastic and plastic anisotropies.

All nanoindentation tests were performed with a sharp Berkovich diamond indenter with a well-calibrated area function [1]. High strain rate impact tests were conducted according to the maximum velocity at impact condition and coil force values F_o of 1, 2, 5, 10, 20, and 50 mN. For comparison, quasistatic tests were performed using the same instrument and indenter tip at constant $\dot{P}/P = 0.05 \text{ s}^{-1}$.

Low-pass Fourier filtering procedures

To illustrate the procedures developed for low-pass Fourier filtering of the raw displacement data to diminish the influences of high-frequency noise, the power spectrum (PSD) of the computed load during an impact test in fused
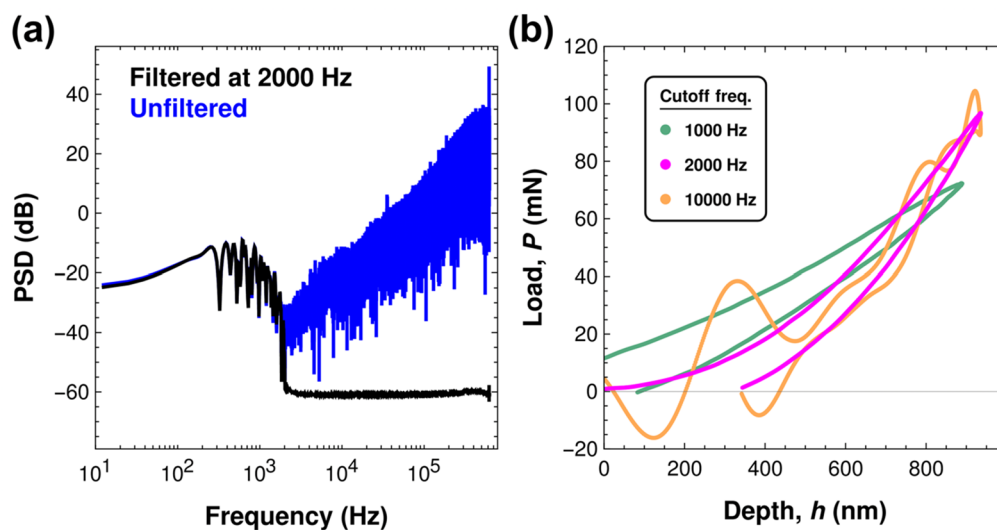
Figure 13: (a) Squared magnitude of the discrete Fourier transform of the computed load on sample for a $F_o = 10$ mN impact test on fused silica shown before (blue) and after (black) applying a low-pass Fourier filter with a cutoff frequency of 2000 Hz, and (b) effect of the cutoff filter frequency on the load–depth curve of the impact test. 1000 Hz is below the optimum cutoff frequency of 2000 Hz and 10,000 Hz is above it.

silica conducted at a coil force of $F_o = 10$ mN is shown in Fig. 13(a). Significant high-frequency noise is plainly visible in the unfiltered case, which obscures the core of the signal residing in the low frequency band below 2000 Hz. The data were treated with a low-pass Fourier filter with the aim of suppressing the high-frequency noise, and thus enabling smooth computation of the derivatives of the displacement–time data. The main parameters defining a low-pass Fourier filter are the frequency cutoff, above which the decomposed frequency amplitudes are attenuated, and the selectivity of the cutoff. The choice of the type of filtering employed here follows from recognizing that any filter will inherently alter the raw signal, but at the same time, high-frequency noise must be removed for usable differentiation. Thus, there is a balancing process in choosing an ideal cutoff frequency. If the cutoff frequency is too high, the data will remain noisy, while if the cutoff frequency is too low, the filter can depress critical frequencies that are important in establishing the real displacement–time response of the material. The choice of cutoff is further complicated by the fact that the frequency response of the sample depends on the mechanical properties of the material and the test conditions [26].

We have found that choosing the cutoff frequency at the minimum in the amplitude trough in the raw data in Fig. 13(a) strikes a good balance and have used this in all our filtering. For the data in Fig. 13(a), a cutoff frequency of 2000 Hz was selected, and applying the filter at this frequency to the displacement data reduces the high-frequency noise levels as indicated in the figure. How the choice of the cutoff frequency affects the derived load–depth curves is shown in Fig. 13(b), where data using cutoffs above (10,000 Hz) and below (1000 Hz) the ideal value (2000 Hz) are all plotted for comparison. Clearly, choosing a frequency higher than the optimally balanced one produces noisy undulations in the curves, and choosing a lower cutoff frequency artificially affects the calculated load at a given depth as evidenced by the shift in 1000 Hz filtered data well above zero load at zero depth.

Acknowledgments

Data availability

The datasets generated and/or analyzed during the current study are available from the corresponding author on reasonable request.

Declarations

Conflict of interest On behalf of all authors, the corresponding author states that there are no conflicts of interest or competing interests.

References

1. W.C. Oliver, G.M. Pharr, Measurement of hardness and elastic modulus by instrumented indentation: advances in understanding and refinements to methodology. J. Mater. Res. **19**, 3 (2004)
2. C.A. Schuh, Nanoindentation studies of materials. Mater. Today **9**, 32 (2006)
3. W.C. Oliver, G.M. Pharr, Nanoindentation in materials research: past, present, and future. MRS Bull. **35**, 897 (2010)
4. G.M. Pharr, Recent advances in small-scale mechanical property testing by nanoindentation. Curr. Opin. Solid State Mater. Sci. **19**, 324 (2015)
5. B. Merle, V. Maier-Kiener, T.R. Rupert, G.M. Pharr, Current trends in nanomechanical testing research. J. Mater. Res. **36**, 2133 (2021)
6. J.E. Field, S.M. Walley, W.G. Proud, H.T. Goldrein, C.R. Siviour, Review of experimental techniques for high rate deformation and shock studies. Int. J. Impact Eng. **30**, 725 (2004)
7. R.W. Klopp, R.J. Clifton, T.G. Shawki, Pressure-shear impact and the dynamic viscoplastic response of metals. Mech. Mater. **4**, 375 (1985)
8. A.C. Mitchell, W.J. Nellis, Shock compression of aluminum, copper, and tantalum. J. Appl. Phys. **52**, 3363 (1981)
9. H. Kolsky, An investigation of the mechanical properties of materials at very high rates of loading. Proc. Phys. Soc. B **62**(11), 676 (1949)
10. R.M. White, Elastic wave generation by electron bombardment or electromagnetic wave absorption. J. Appl. Phys. **34**(7), 2123 (1963)
11. C. Zehnder, J.N. Peltzer, J.S.K.L. Gibson, S. Korte-Kerzel, High strain rate testing at the nano-scale: a proposed methodology for impact nanoindentation. Mater. Des. **151**, 17 (2018)
12. L. Qin, H. Li, X. Shi, B.D. Beake, L. Xiao, J.F. Smith, Z. Sun, J. Chen, Investigation on dynamic hardness and high strain rate indentation size effects in aluminium (110) using nano-impact. Mech. Mater. **133**, 55 (2019)

13. M. Rueda-Ruiz, B.D. Beake, J.M. Molina-Aldareguia, New instrumentation and analysis methodology for nano-impact testing. Mater. Des. **192**, 108715 (2020)

14. G. Guillonneau, M. Mieszala, J. Wehrs, J. Schwiedrzik, S. Grop, D. Frey, L. Philippe, J.M. Breguet, J. Michler, J.M. Wheeler, Nanomechanical testing at high strain rates: new instrumentation for nanoindentation and microcompression. Mater. Des. **148**, 39 (2018)

15. P. Sudharshan Phani, W. Oliver, Ultra high strain rate nanoindentation testing. Materials (Basel) **10**, 663 (2017)

16. B. Merle, W.H. Higgins, G.M. Pharr, Extending the range of constant strain rate nanoindentation testing. J. Mater. Res. **35**, 343 (2020)

17. D. Tabor, A simple theory of static and dynamic hardness. Proc. R. Soc. Lond. A **192**, 247 (1948)

18. R.M. Davies, The determination of static and dynamic yield stresses using a steel ball. Proc. R. Soc. Lond. A **197**, 416 (1949)

19. M. Hassani, D. Veysset, K.A. Nelson, C.A. Schuh, Material hardness at strain rates beyond 10^6 s^{-1} via high velocity microparticle impact indentation. Scr. Mater. **177**, 198 (2020)

20. A.W. Crook, A study of some impacts between metal bodies by a piezo-electric method. Proc. R. Soc. Lond. A **212**, 377 (1952)

21. C.H. Mok, J. Duffy, The dynamic stress–strain relation of metals as determined from impact tests with a hard ball. Int. J. Mech. Sci. **7**, 355 (1965)

22. J. Nobre, A. Dias, R. Gras, Resistance of a ductile steel surface to spherical normal impact indentation: use of a pendulum machine. Wear **211**, 226 (1997)

23. G. Subhash, B.J. Koepple, A. Chandra, Dynamic indentation hardness and rate sensitivity in metals. J. Eng. Mater. Technol. Trans. ASME **121**, 257 (1999)

24. J. Lu, S. Suresh, G. Ravichandran, Dynamic indentation for determining the strain rate sensitivity of metals. J. Mech. Phys. Solids **51**, 1923 (2003)

25. M.J. Mayo, W.D. Nix, A micro-indentation study of superplasticity in Pb, Sn, and Sn–38 wt% Pb. Acta Metall. **36**, 2183 (1988)

26. P. Sudharshan Phani, B.L. Hackett, C.C. Walker, W.C. Oliver, G.M. Pharr, On the measurement of hardness at high strain rates by nanoindentation impact testing. J. Mech. Phys. Solids **170**, 105105 (2023)

27. W.C. Oliver, G.M. Pharr, An improved technique for determining hardness and elastic modulus using load and displacement sensing indentation experiments. J. Mater. Res. **7**, 1564 (1992)

28. B.N. Lucas, W.C. Oliver, Indentation power-law creep of high purity indium. Metall. Trans. A **30**, 601 (1999)

29. A. Bolshakov, G.M. Pharr, Influences of pile-up on the measurement of mechanical properties by load and depth sensing indentation techniques. J. Mater. Res. **13**, 1049 (1998)

30. G.M. Pharr, E.G. Herbert, Y.F. Gao, The indentation size effect: a critical examination of experimental observations and mechanistic interpretations. Annu. Rev. Mater. Res. **40**, 271–290 (2010)